Empirical Investigations of the Instrument Response for Distributed Acoustic Sensing (DAS) across 17 Octaves

Patrick Paitz*[1], Pascal Edme[1], Dominik Gräff[2], Fabian Walter[2], Joseph Doetsch[1], Athena Chalari[3], Cédric Schmelzbach[1], and Andreas Fichtner[1]

ABSTRACT

With the potential of high temporal and spatial sampling and the capability of utilizing existing fiber-optic infrastructure, distributed acoustic sensing (DAS) is in the process of revolutionizing geophysical ground-motion measurements, especially in remote and urban areas, where conventional seismic networks may be difficult to deploy. Yet, for DAS to become an established method, we must ensure that accurate amplitude and phase information can be obtained. Furthermore, as DAS is spreading into many different application domains, we need to understand the extent to which the instrument response depends on the local environmental properties. Based on recent DAS response research, we present a general workflow to empirically quantify the quality of DAS measurements based on the transfer function between true ground motion and observed DAS waveforms. With a variety of DAS data and reference measurements, we adapt existing instrument-response workflows typically in the frequency band from 0.01 to 10 Hz to different experiments, with signal frequencies ranging from 1/3000 to 60 Hz. These experiments include earthquake recordings in an underground rock laboratory, hydraulic injection experiments in granite, active seismics in agricultural soil, and icequake recordings in snow on a glacier. The results show that the average standard deviations of both amplitude and phase responses within the analyzed frequency ranges are in the order of 4 dB and 0.167π radians, respectively, among all experiments. Possible explanations for variations in the instrument responses include the violation of the assumption of constant phase velocities within the workflow due to dispersion and incorrect ground-motion observations from reference measurements. The results encourage further integration of DAS-based strain measurements into methods that exploit complete waveforms and not merely travel times, such as full-waveform inversion. Ultimately, our developments are intended to provide a quantitative assessment of site- and frequency-dependent DAS data that may help establish best practices for upcoming DAS surveys.

KEY POINTS

- We empirically quantify the instrument response of DAS for experiments spanning 17 octaves in frequency.
- Based on comparison to conventional sensors, the DAS response is consistent over the investigated frequencies.
- The results of this study encourage further integration of DAS measurements into geophysical workflows.

Supplemental Material

INTRODUCTION

Distributed acoustic sensing (DAS) is a method to utilize an optical fiber as an instrument to measure strain or strain rate along the fiber. Following successful early DAS applications in border and pipeline monitoring and as downhole seismic instruments in the seismic exploration industry, the method was recently adopted in longer-period seismology (Daley *et al.*, 2013; Li *et al.*, 2015; Hartog, 2017; Martin *et al.*, 2017).

With the benefit of high temporal and dense spatial sampling even in remote areas, and the potential to use existing fiber-optic infrastructure, for example, in urban areas, DAS

1. Department of Earth Sciences, Institute of Geophysics, ETH Zürich, Zürich, Switzerland; 2. Laboratory of Hydraulics, Hydrology and Glaciology, ETH Zürich, Zürich, Switzerland; 3. Silixa Ltd., Elstree, Hertfordshire, United Kingdom

*Corresponding author: patrick.paitz@erdw.ethz.ch

Cite this article as Paitz, P., P. Edme, D. Gräff, F. Walter, J. Doetsch, A. Chalari, C. Schmelzbach, and A. Fichtner (2020). Empirical Investigations of the Instrument Response for Distributed Acoustic Sensing (DAS) across 17 Octaves, *Bull. Seismol. Soc. Am.* **111**, 1–10, doi: 10.1785/0120200185

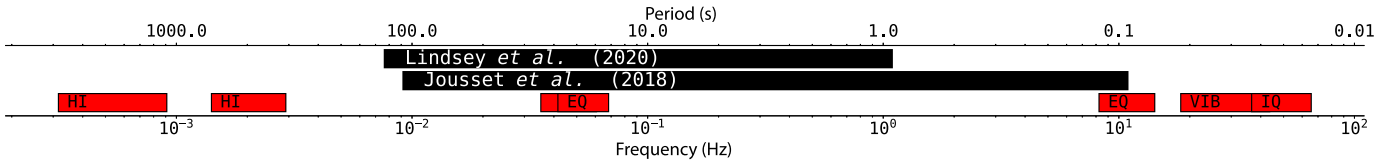

Figure 1. Overview of the frequencies covered by the experiments in this article, in context to existing instrument-response studies of distributed acoustic sensing (DAS) (black). The instrument-response study covers hydraulic injection experiments (denoted HI), earthquake recordings (denoted EQ), active vibroseis shots (denoted VIB), and icequake recordings (denoted IQ). The color version of this figure is available only in the electronic edition.

is in the process of revolutionizing seismic and seismological data acquisition on multiple scales across the Earth. However, the quality of DAS measurements for seismological applications needs further quantitative assessments. In addition to site and orientation effects due to limited broadside sensitivity of DAS along straight fibers (Kuvshinov, 2016), data quality is affected by the transfer function between the deforming medium (i.e., the Earth) and the fiber, which, in turn, depends on fiber coupling and cable properties. Optical noise also influences the quality of the DAS measurement and is further discussed in Lindsey *et al.* (2020).

The quality of DAS measurements, as compared with more traditional instrumentation, has been the focus of numerous recent works ranging from very long periods of several hours in laboratory environments (Becker and Coleman, 2019) to ambient noise studies (Martin *et al.*, 2016, 2018; Dou *et al.*, 2017) and earthquake detection (Lindsey *et al.*, 2017; Wang *et al.*, 2018; Ajo-Franklin *et al.*, 2019) to active-source seismic experiments (Daley *et al.*, 2013). Most studies have not gone through the rigorous step of quantifying an instrument reponse function, though initial responses were presented in Jousset *et al.* (2018) (0.1–100 s period) and Lindsey *et al.* (2020) (1–120 s period). These existing analyses of the DAS response function are typically in a limited part of the frequency band from 0.01 to 10 Hz and are based on comparisons with well-coupled conventional seismometers for which the instrument response is sufficiently well known to be removed from the signal (Lindsey *et al.*, 2020). Whereas Jousset *et al.* (2018) investigate the strain instrument response theoretically and compare displacement spectra of (corrected) DAS recordings with displacement recordings of a broadband seismometer and a geophone, Lindsey *et al.* (2020) shows the first comprehensive empirical instrument-response study in which DAS data are converted to velocity in the f-k domain and then compared with recordings of a broadband seismometer.

One potential of DAS, however, is to cover a much broader range of frequencies than any other instrument previously, and most of these existing studies were restricted to a given application and frequency range.

In this study, we extend the existing analyses in the frequency band from 1/120 to 10 Hz to an instrument-specific DAS response of the Silixa iDAS, covering a frequency range of more than 17 octaves, from around 0.3 mHz to 60 Hz. This is based on a series of experiments, including (1) low-frequency strain induced by hydraulic injection in a borehole with collocated fiber-Bragg-grating (FBG) strainmeters, (2) local-to-teleseismic earthquake recordings with a collocated broadband seismometer station, (3) active controlled-source experiments with collocated geophones, and (4) stick-slip icequake recordings with collocated seismometers on a glacier.

The frequencies covered in this article, as well as the frequencies covered in the work by Jousset *et al.* (2018) and Lindsey *et al.* (2020), are visualized in Figure 1. For all experiments, collocated instruments with known response functions were installed to obtain estimates of ground motion for comparison and quantification of the DAS response.

This article is organized as follows: In the Instrument Response Estimation section, we introduce the necessary theory for instrument-response and gradient-wavefield observations in the context of DAS seismology. The Experiment Overview section contains an overview of the DAS experiments discussed in this study and a summary of the data processing workflow. The resulting instrument-response curves and example waveforms are then shown in the Results section and further discussed in the Discussion section, with an emphasis on current and future applications of DAS for subsurface monitoring.

INSTRUMENT-RESPONSE ESTIMATION

Estimates of the effective DAS instrument response require two main ingredients: (1) A collocated instrument with known response, and (2) a conversion of the measurements into the same physical quantity, which is most commonly displacement in the direction of the fiber. In the following sections, we elaborate on these two ingredients. We follow the derivations of Daley *et al.* (2016), Wang *et al.* (2018), and Lindsey *et al.* (2020).

Comparison with collocated reference measurements

Assuming sufficiently small displacements, the ith component of an observed displacement waveform $\mathbf{u}(\mathbf{x}, \omega)$ at the point location $\mathbf{x}$ and circular frequency ω can be expressed in terms of true ground deformation $\mathbf{g}(\mathbf{x}, \omega)$ and a linear transfer operator or instrument response $\mathbf{T}(\omega)$:

$$u_i(\mathbf{x}, \omega) = \sum_{j=1}^{3} T_{ij}(\omega) g_j(\mathbf{x}, \omega), \quad (1)$$

in which j is the component of ground deformation in some suitable 3D coordinate system. The off-diagonal elements of $\mathbf{T}$ describe the mostly undesirable mapping of components into each other, and they may be nonzero, for instance, when an instrument is misoriented or the Poisson effect of a fiber-optic cable in the case of a DAS acquisition system is significant. While being of general interest, the complete set of transfer tensor elements is not accessible with DAS measurements along a straight cable, because the measurements are confined to the cable direction, described by the unit vector $\mathbf{e}(\mathbf{x})$. Hence, we are forced to base our analysis on an approximate scalar version of equation (1):

$$u_e(\boldsymbol{x}, \omega) = T_e(\omega) g_e(\boldsymbol{x}, \omega), \tag{2}$$

with the projections $u_e = \mathbf{u}^T\mathbf{e}$ and $g_e = \mathbf{g}^T\mathbf{e}$. The estimation of the scalar instrument response is possible when collocated measurements $u_e^{'}$ with known instrument response $T_e^{'}$ are available. For example, we might use $u^{'}$ and $T^{'}$ to refer to the observations and response of a known broadband instrument that we use for comparison. Solving

$$u_{e^{'}}(\mathbf{x}, \omega) = T_e^{'}(\omega) g_e(\mathbf{x}, \omega), \tag{3}$$

for g_e and inserting into equation (2), yields

$$T_e(\omega) = T_{e^{'}}(\omega) \frac{u_e(\mathbf{x}, \omega)}{u_{e^{'}}(\mathbf{x}, \omega)} = T_{e^{'}}(\omega) \frac{u_e(\mathbf{x}, \omega) u_{e^{'}}^{*}(\mathbf{x}, \omega)}{|u_{e^{'}}(\mathbf{x}, \omega)|^2}, \tag{4}$$

in which $*$ denotes complex conjugation. To prevent division by small numbers, it is important to limit the instrument-response estimation to frequencies for which the power spectra of both observations are significantly nonzero or to add a waterlevel to the denominator in equation (4).

Conversion of observed quantities

Equation (4) rests on the assumption that u_e and $u_{e^{'}}$ are identical physical quantities. Because most of our collocated reference measurements are velocity recordings, the DAS measurements of strain or strain rate, therefore, need to be converted.

The output quantity of DAS measurements depends on the interrogator. For this study, we use the Silixa iDAS that measures strain rate. Within a few meters of the DAS interrogator, and depending on the specific experiment (see the Experiment Overview section), we performed reference measurements using either an FBG strain sensor, geophones, or seismometers measuring ground velocity.

Strain ε_e in the direction $\mathbf{e}(\mathbf{x})$ of the fiber can be expressed in terms of the displacement field $\mathbf{u}(\mathbf{x}, \omega)$ as

$$\varepsilon_e(\mathbf{x}, \omega) = \sum_{i,j=1}^{3} e_i(\mathbf{x}) \frac{1}{2} \left(\frac{\partial u_i(\mathbf{x}, \omega)}{\partial x_j} + \frac{\partial u_j(\mathbf{x}, \omega)}{\partial x_i} \right) e_j(\mathbf{x}). \tag{5}$$

In general, DAS measurements are averages over an interval along the fiber called the gauge length γ (Daley *et al.*, 2016). This largely controls spatial resolution and the signal-to-noise ratio (SNR). As the apparent wavelength λ of the incident wave approaches γ, the measurement of averaged strain is significantly different from the actual strain. In our experiments, the minimum apparent wavelength is on the order of 50–100 m. Because this is large compared with the 10 m gauge length of the iDAS, the averaging effect can safely be ignored.

Invoking plane-wave decomposition, the relationship between strain ε_e and particle velocity $v_e = du_e/dt$ can be expressed as (Daley *et al.*, 2016; Wang *et al.*, 2018)

$$\varepsilon_e(\mathbf{x}, \omega) = \frac{1}{c(\mathbf{x}, \omega)} v_e(\mathbf{x}, \omega), \tag{6}$$

in which c is the apparent phase velocity along the cable direction, defined in terms of wavenumber k and frequency ω, as $c = \omega/k$. The apparent phase velocity depends on frequency, incidence angle, and subsurface properties in the vicinity of the measurement location $\boldsymbol{x}$. Under the assumption of a single plane wave, the conversion of strain to particle velocity or vice versa can either be performed in the time domain for any known c or by rescaling in the frequency–wavenumber (f-k) domain (Wang *et al.*, 2018). For the comparison between DAS and geophone or seismometer data, we integrate DAS data from strain rate to strain and then convert to velocity in the time domain using apparent phase-velocity estimates. The FBG sensors used in our experiments measure strain directly, and hence integrated DAS data from strain rate to strain can be compared directly with these measurements.

Recent experiments have shown that conversion in the f-k domain may be more accurate (Wang *et al.*, 2018). However, this was not possible in our case due to the narrow wavenumber content in our individual experiments. In addition, when analyzing data with narrow wavenumber content, the introduction of a waterlevel is required in f-k domain conversion (Lindsey *et al.*, 2020). This waterlevel may have a strong effect on the phase velocity and may, therefore, yield an unphysical modification. Finally, because the exact physical collocation of two instruments is not possible, site effects together with imperfect fiber-to-ground coupling can influence the measurement as well.

EXPERIMENT OVERVIEW

In the following, we describe the individual narrowband experiments that contribute to the final broadband instrument response. This includes information on the experimental setup, the data processing, and the instrument-response estimation. A more detailed and technical description of the cable installations and the investigated signals is summarized in Table A1.

Experiment location and instrumentations

To analyze instrument responses of DAS in a wide frequency range and under different conditions, we conducted a series of

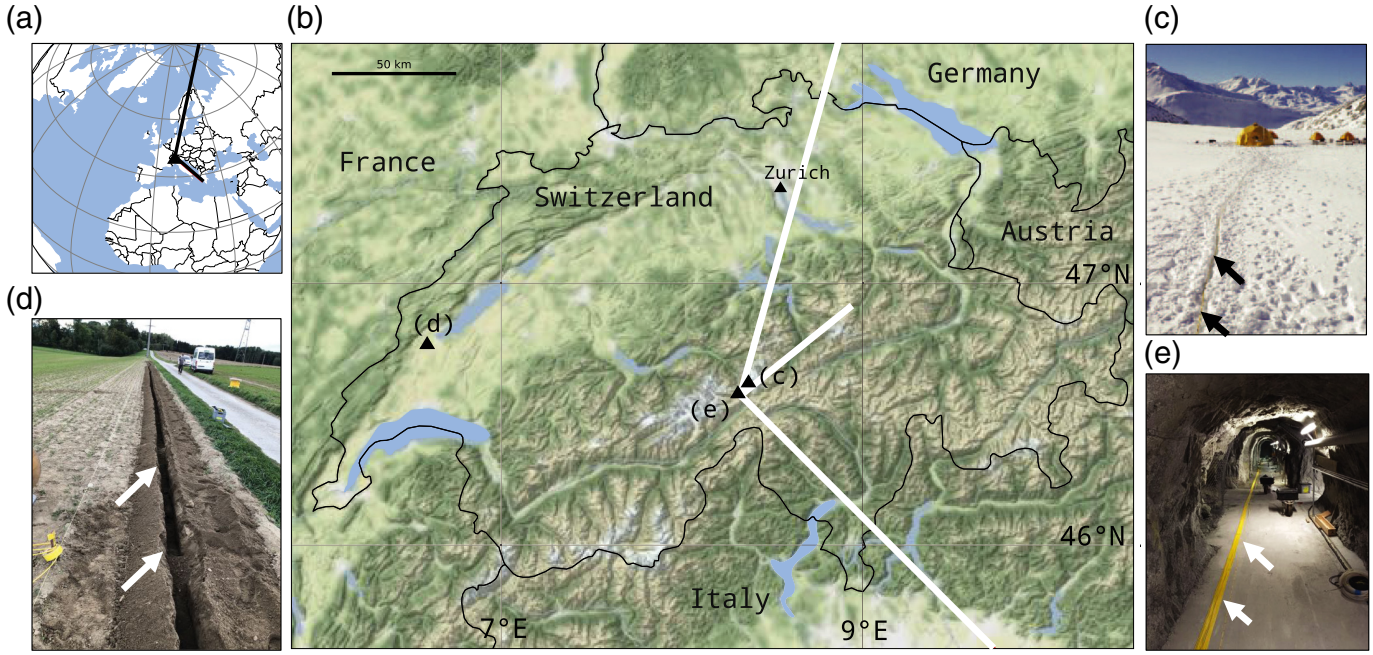

Figure 2. The geographic location of the individual experiments is shown in (a,b), indicated by the triangles. Experimental conditions are shown in (c) for the Rhonegletscher icequake recording, in (d) for the active seismics field test in western Switzerland close to Yverdon-les-Bains, and in (e) for the Grimsel test site (GTS) earthquake recordings. Lines in (a,b) show the back azimuths of the surface waves for the earthquake recordings at the GTS (black and white, respectively). Arrows point to the installed cable (c,e) and to the trench in which the cable was installed (d). Arrows in (c–e) are approximately 1 m apart. In addition to the cable visible for the GTS in (e), a borehole installation at the same test site was used for the hydraulic stimulation experiment. Panel (c) is adapted after Walter *et al.* (2020). The color version of this figure is available only in the electronic edition.

active and passive experiments in different settings: (1) active hydraulic stimulation experiments between 1/3600 and 1/200 Hz at the Grimsel test site (GTS) rock laboratory in the Swiss Alps (Doetsch *et al.*, 2018; Krietsch *et al.*, 2018) with collocated Micron Optics Inc. os3600 FBG sensors, (2) passive earthquake recordings between 1/26 and 13 Hz in a tunnel within the GTS rock laboratory with a collocated Streckeisen STS2 seismometer (Quanterra Q330HRS digitizer), (3) active-source seismics with signals between 20 and 40 Hz on an agricultural field near the city of Yverdon-les-Bains in western Switzerland and collocated INPUT/OUTPUT INC. SM6 (14 Hz) geophones (Geometrics ES-3000 digitizer), and (4) passive icequake recordings between 40 and 60 Hz on Rhonegletscher, a temperate glacier in the Swiss Alps, with a collocated three-component Lennartz 3D/BHs sensor (Nanometrics Centaur digitizer). A detailed description of the experiment on Rhonegletscher can be found in Walter *et al.* (2020). An overview on the locations of the experiments is shown in Figure 2.

The fiber installation and environmental conditions strongly varied among the various experiments. Whereas the cable was cemented in a 40-meter-deep borehole for the hydraulic-stimulation experiment (1), it was just loosely lying on the ground for the GTS passive earthquake recordings (3) in a 60-meter-long tunnel, looping back and forth with some parts of the cable covered by gravel bags (over a 10 m section), some parts taped to the ground (over a 10 m section), and some parts of the cable covered with wooden blocks (over a 10 m section). For the active seismics (2), the cable was trenched in soil at a depth of approximately 10 cm over a length of 100 m and for the icequake recordings (4), the fiber-optic cable was trenched in snow at a depth of between 2 and 10 cm.

Workflow and data processing

Preprocessing, apparent phase-velocity estimation, and conversion. We preprocessed the data recorded in the various experiments before estimating the instrument response. This included de-trending and tapering, the integration of iDAS data from strain rate to strain, and finally the application of a Butterworth band-pass filter. The filter frequencies are specified in Table A1.

With the exception of the long-period experiment at the GTS, with collocated FBG strain sensors, strain from DAS measurements had to be converted to velocity to ensure comparability of DAS and collocated velocity data. As explained in the Conversion of Observed Quantities section, the most suitable conversion approach for our experiments is rescaling with an estimated apparent phase velocity. In addition to avoiding potential numerical instabilities of f-k-domain rescaling, the approach is numerically robust, and it enables a channel-by-channel instrument-response analysis.

For the GTS experiments, we look at a range of earthquakes from various distances and frequencies. For the teleseismic and

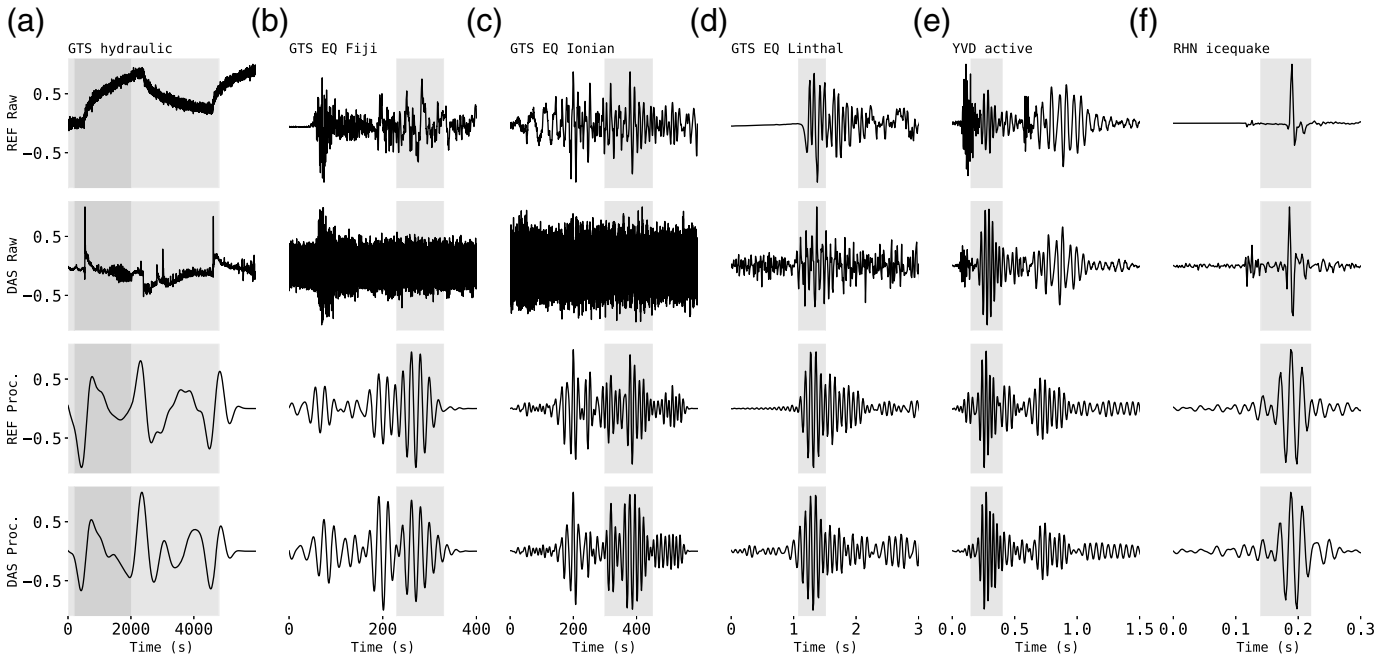

Figure 3. Normalized waveforms (with respect to maximum amplitude) of raw reference data (top row, denoted REF Raw), raw DAS data (second row, denoted DAS Raw), processed reference data (third row, denoted REF Proc.), and processed and converted DAS data (fourth row, denoted DAS Proc.). (a) The first column shows the waveforms for the hydraulic stimulation experiment in the boreholes at the GTS (GTS, fiber-Bragg-grating, and DAS data). (b–d) The second to fourth columns show earthquake recordings from the tunnel installation at GTS (seismometer and DAS data). (e) The fifth column shows waveforms from the active seismic experiment in Yverdon-les-Bains (YVD, geophone and DAS data), and (f) the last column visualizes icequake recordings from the Rhonegletscher (RHN, seismometer and DAS data). The raw reference data (REF Raw) is always raw velocity data, except for the hydraulic injection (HI), in which it is strain. The raw DAS data (DAS raw) is the recorded raw strain-rate signal. The processed waveforms are in the unit of velocity, except for the HI, in which the processed waveforms are strain waveforms. Gray boxes indicate the signal window for which we estimated the instrument response. Two different gray boxes in (a) indicate two different signal windows used for different frequency bands of the instrument response. Because this summary plot is primarily intended to show overall similarities and differences, we present enlarged versions of each subplot in Figures S1–S6. The detailed instrument descriptions for the reference data are available in Table A1.

regional earthquake recordings (distances of 16,000 and 1300 km and denoted EQ Fiji and EQ Ionian, respectively) at the GTS, with frequencies around 0.05 Hz, we use a Rayleigh-wave phase velocity of 3.6 km/s, typical for the Alpine region (Fry *et al.*, 2010), and around 10% lower than the global continental average (Dziewoński *et al.*, 1975). The local event (distance of 60 km, denoted EQ Linthal) has a dominant frequency of around 10 Hz, corresponding to wavelengths of a few hundred meters. We, therefore, work with a Rayleigh-wave phase velocity calculated for a homogeneous half-space with S velocity of 3000 m/s, typical for granite at the GTS. After calculating the back azimuth of the surface wave, we used the Rayleigh-wave window to calculate the apparent phase velocity.

For the Yverdon-les-Bains active-source experiment, the phase velocity was estimated from a seismic section by comparing the arrival times of the high-amplitude surface wave for the first and last DAS cable channel. This gave a phase velocity along the cable of 1200 m/s for the surface-wave arrival with the largest amplitude.

It was difficult to obtain a phase-velocity estimate for the icequake recording of the Rhonegletscher experiment. We picked an apparent phase velocity of a seismic section of only 10 DAS channels and obtained an estimated apparent phase velocity of 5500 m/s for the direct S-wave arrival.

The phase-velocity estimates required for the conversion from strain to velocity are apparent phase velocities along the fiber for specific seismic phases. The windows indicated in Figure 3, for which we estimated DAS instrument responses, are chosen for their high SNR, with the additional constraint to minimize overlap with other arrivals with potentially different apparent phase velocities. An incorrect estimate of apparent phase velocity affects the estimated amplitude response, but not the phase response of the DAS. This is further discussed in the Possible Causes of Instrument Response Variations section.

Instrument-response estimation. After preprocessing, we estimate a site-specific instrument response of the DAS system using equation (4) within an appropriate frequency range in which recorded power spectra are signficantly nonzero. To analyze the instrument response, we consider its amplitude and phase independently. To avoid complications with phase unwrapping, we note that the phase of $T_e(\omega)$ is typically the small phase difference between the converted DAS recording

$u_e(\omega)$ and the ground motion $g_e(\omega)$, estimated from equation (2). This phase difference can be conveniently computed from the correlation of $u_e(\omega)$ and $g_e(\omega)$.

Beacuse DAS measurements record ground motion on numerous closely spaced channels, we compute a DAS response for every channel individually. Ideally, there would be a collocated measurement of ground motion available for every DAS channel, but, in reality, this is not feasible. Instead, we often have to rely on a single reference measurement in the vicinity of a DAS array. This is legitimate when the distance between each DAS channel and the reference measurement is only a fraction of the wavelength, and the medium in which the instruments are installed have the same properties. In our experiments, this was generally the case. If the interrogated fiber had homogeneous backscattering properties and identical coupling with exact physical collocation, all investigated DAS channels had an identical response function. Because this is not met in reality, we will compare all available DAS channels.

RESULTS

Time-domain waveforms

To illustrate the effect of the preprocessing and conversion, Figure 3 shows a selection of time-domain DAS and reference waveforms from each of the experiments described in the Experiment Overview section. The examples are representative of the more general observation that the main features of reference and preprocessed DAS measurements are visibly similar, whereas the corresponding raw recordings may have little in common. This is more quantitatively reflected in the unnormalized cross-correlation coefficients between raw reference and DAS data, which range between 0.01 and 0.08 (absolute correlation coefficient). In contrast, the correlation coefficient for the processed data ranges between 0.78 and 0.95 for the examples shown in Figure 3.

Despite the similarities of processed reference and DAS waveforms, there are obvious small differences between them. To investigate them in more detail, we analyze frequency-dependent instrument responses for the events from Figure 3 in the following section.

Instrument-response curves

The estimated instrument responses for all available DAS channels, including the few examples from Figure 3, are visualized in Figure 4. For readability, the range of the instrument-response functions within the standard deviations and the mean values of amplitude and phase response are plotted in each subfigure. In addition, the minimum and maximum values of the response curves are plotted as well. If the DAS data were exactly ground-motion measurements, the instrument-response curves in Figure 4 would show flat horizontal lines at 0 dB and 0 rad, respectively. Each of the subplots in Figure 4 visualizes a collection of effective instrument-response curves for each DAS experiment in a certain frequency band and at a specific site.

The number of available DAS and reference measurements depends on the site and the experimental setup. For the hydraulic injection experiment, for instance, we could compare only two DAS channels with two separate collocated FBG measurements. For the GTS tunnel recordings, we compared 206 and 250 DAS channels, respectively, with one nearly collocated seismometer. The maximum distance between seismometer and DAS channels at the GTS is 50 m. With 15 DAS channels and almost exactly collocated geophones, we compared the data from Yverdon-les-Bains channel by channel. In the response analysis from Rhonegletscher, we used two DAS channels in the vicinity of a single seismometer, with a maximum distance of 10 m. The number of available sufficiently collocated channels is limited by the receiver layout and the wavelength.

From Figure 4, we observe that instrument responses vary in both amplitude and phase. Across frequency bands, the mean amplitude response varies between −12.45 (GTS Fiji earthquake recording) and 10.42 dB (Rhonegletscher icequake recording). Mean phase responses range from -0.06π (GTS hydraulic stimulation experiment) to 0.04π rad (GTS Linthal earthquake recording). Excluding experiments with only two DAS measurements, the standard deviation of the amplitude response is on the order of 4 dB. For the effective phase responses, the standard deviations range from 0.035π rad for the GTS earthquake recording in (d) to 0.36π rad for the GTS earthquake recording in (e). The average standard deviations of amplitude and phase response among all experiments are 4.0 dB and 0.17π rad, respectively.

DISCUSSION

The most important result of this work is the observation that, despite all sources of errors and differences in experimental setups, the DAS amplitude response only varies by around ±10 dB over a frequency range from 1/2900 to 60 Hz, that is, over more than 17 octaves. The phase response is typically on the order of 0.1π. In the following sections, we discuss possible reasons for the instrument-response variations, as well as implications for current and future applications. Comparing the results with the instrument-response curves in Lindsey *et al.* (2020) for the frequency range from 1/120 to 1 Hz, we find a instrument response that is up to 10 dB lower. The authors in Lindsey *et al.* (2020) stack data over five gauge lengths (10 m), whereas our results are channel by channel.

Possible causes of instrument-response variations

Although deviations of the instrument response from a flat response might be a property of the DAS interrogator itself, they are more likely to result from assumptions and approximations used during the approximation procedure.

The variations of the amplitude response within and across experiments may be related to incorrect phase-velocity

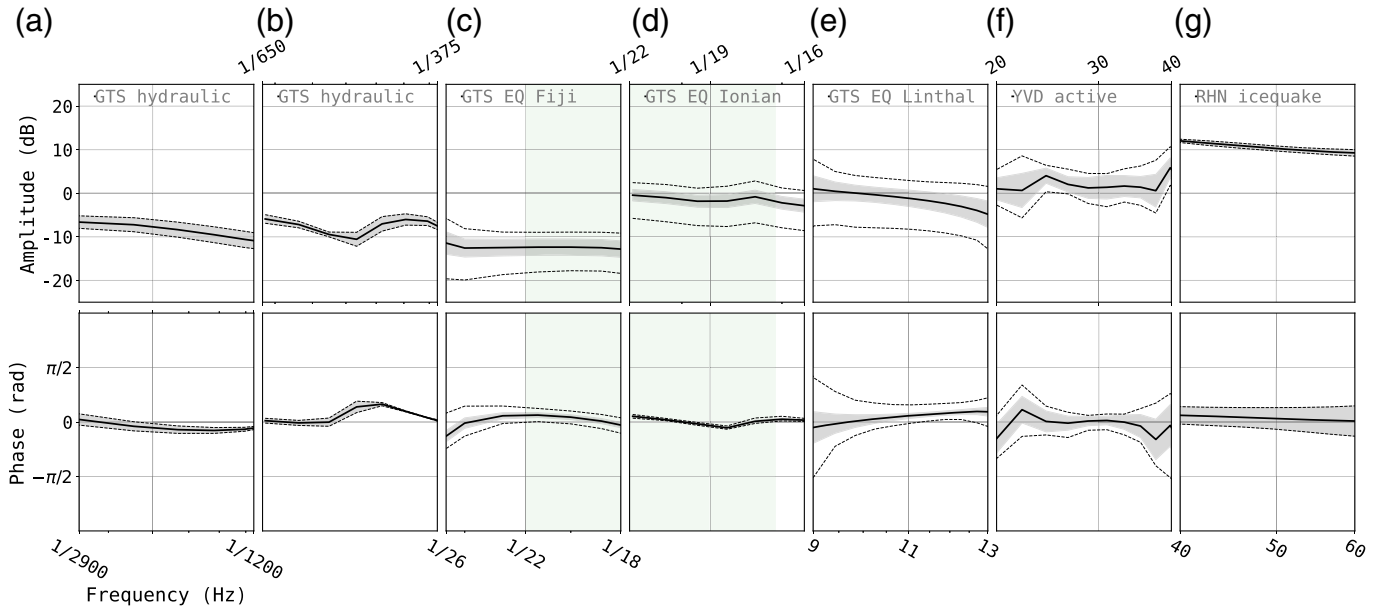

Figure 4. Summary of estimated instrument responses for all experiments. The top row shows the amplitude responses in dB as DAS ground motion with respect to ground motion from reference measurements (20 $\log_{10}$ of the ratio between DAS spectrum and the spectrum of the ground motion), and the bottom row shows the phase responses as phase difference between DAS ground motion and ground motion from reference measurements in radians. (a,b) Columns correspond to different frequency ranges covered by the hydraulic stimulation experiment, (c–e) earthquake recordings at the GTS, (f) the active experiment near YVD, and (g) the icequake on RHN. Black lines in the center indicate the mean amplitude and phase responses from all available DAS channels, and the gray-shaded area around the mean represents the corresponding standard deviation. Black dashed lines indicate the minimum and maximum instrument-response values. The shaded area between (c) and (d) indicates an overlap in frequencies between the two columns. The number of DAS channels is $n = 2$ for (a) and (b), $n = 250$ for (c) and (e), $n = 206$ for (d), $n = 15$ for (f), and $n = 2$ for (g). (Clearly, the standard deviation for $n = 2$ has limited meaning.) For the investigated signals, if the DAS data were recordings of true ground motion, both amplitude and phase response should be horizontal lines at 0 dB and 0 rad, respectively. For details on the instrumentation, see Table A1 and for a larger image of each subfigure with more details, see the supplemental material. The color version of this figure is available only in the electronic edition.

estimates. Largely owing to the small size of the DAS arrays used in this study, the DAS data conversion via equation (6) is based on a frequency-independent phase velocity for each frequency band. Within the relatively narrow frequency bands of the individual experiments, one may expect phase-velocity variations on the order of 10%, which translates to amplitude response errors of around 1 dB. This is sufficient to explain amplitude response variations at the GTS.

The small standard deviation of the amplitude response within the individual experiments indicates that the details of cable-to-ground coupling play a relatively minor role, as long as the cable is shielded from wind. This is particularly evident for the surface-cable experiment in the GTS tunnel. Though different cable segments were coupled very differently (i.e., not at all, glued to the surface with tape, weighted with wooden blocks, or sand bags), the standard deviation of the amplitude response is typically around 1 dB, that is, around 10%.

An additional source of error are inaccuracies of the instrument responses in the reference measurements. This seems to be the most plausible explanation of the strong response variations at the Yverdon-les-Bains test site, where each DAS channel is compared with a separate geophone and is the subject of further ongoing research.

An outlier in the response analysis is the Rhonegletscher experiment. A possible explanation of the strong overestimation of the amplitude response is a local site effect or imperfect collocation. In fact, we performed the reference measurement on ice below a snow cover of about 2 m, whereas the DAS cable was located on the snow surface, which has different elastic properties that could potentially result in amplitude amplifications similar to amplifications in sedimentary basins.

We also calculated the SNR, defined as the ratio of root mean square amplitudes of the indicated signal windows and the root mean square amplitude of a manually picked noise window of the same length for every DAS channel individually. We did this for all experiments, except for the hydraulic injection experiment in which picking a noise window was not possible, and for the Fiji earthquake recording in which the trimmed data were too short to pick a large enough noise window. The mean SNR of the DAS data ranges from 6.3 for the active seismic experiment to 15.1 for the Linthal earthquake recordings, whereas the mean SNR of the reference instruments ranges from 6.1 for the Ionian Sea earthquake recordings to 19.6 for the Linthal earthquake recordings. There seems to be no obvious connection between the SNR and the instrument-response values for the investigated signals.

Finally, and in addition to the previously mentioned factors, subwavelength heterogeneities may contribute to an effective instrument response for strain measurements that are not perfectly flat (Singh *et al.*, 2019). Given that (1) phase-velocity errors only account for around 1 dB in amplitude response, (2) the amplitude response variations vary smoothly with frequency, and (3) cable-to-ground coupling seems to play a minor role, one may hypothesize that subwavelength heterogeneities play a significant role.

Implications for current and future applications

The frequency bandwidth of the DAS instrument response enables applications ranging from mHz in normal-mode seismology to several tens of Hz in seismic exploration and seismic hazard analysis.

This would be particularly attractive for environmental seismology, as a broad spectrum of phenomena may be captured with a single instrument. These phenomena include long-period temperature variations, precipitation, induced seismicity, mass movement, and subsurface velocity changes due to natural or anthropogenic activity.

In fact, the potential of DAS in seismic hazard analysis largely derives from the co-use of existing telecommunication cables. The comparatively small effect of cable-to-ground coupling makes applications that leverage existing fiber infrastructure more viable. The most likely, and closely related, bottlenecks are unknown subwavelength structure and reliable phase-velocity estimates. These may hinder accurate conversions from strain to displacement or velocity amplitudes and later to ground-motion proxies such as spectral acceleration or peak ground acceleration. This may be overcome by incorporating strain observations into seismic hazard frameworks.

The small phase response of the DAS system enables travel-time measurements with an error typically below 5% of the dominant period. To put this in perspective: in the case of the local Linthal event (Fig. 4a), the travel-time error would result in an error of 0.025% of the estimated Rayleigh-wave velocity along the path from source to receiver. Because corresponding numbers are similar for other examples, this suggests that seismic tomography based on DAS travel-time measurements is entirely feasible, even without instrument-response removal. This is also shown theoretically for apparent wavelengths exceeding the gauge length, for example, in the supplementary material of Walter *et al.* (2020).

To reduce errors in tomographic images (and other inferences), it is certainly advisable to avoid strain-to-displacement or strain-to-velocity conversions, typically based on a plane-wave assumption. This is particularly important for future DAS-based waveform and finite-frequency tomography, as envisioned, for instance, by Paitz *et al.* (2018). A prerequisite would be the integration of strain into standard seismological workflows and processing tools.

Finally, we note that DAS instrument-response studies, as the one presented here, could of course be improved. To better estimate apparent phase velocities, a spatial sampling that can resolve all expected apparent wavelengths is important. This can be accomplished by sufficiently long fibers for larger wavelengths, and by sufficiently fine spatial sampling and gauge lengths for signals of small wavelengths. Combining multiple gauge lengths has the potential to improve multiscale fiber-optic seismology in the future. Furthermore, fibers oriented in multiple directions may help overcome the limited broadside sensitivity of DAS and to better estimate phase velocities for waves traveling along different fiber sections. An example of this would be helically wound fibers, as for example, described in Kuvshinov (2016). Though coupling of the fiber seems to have a small effect for the experiments considered here, the influence of coupling on the SNR and repeatability certainly requires further investigation.

CONCLUSIONS AND OUTLOOK

We investigated the amplitude and phase response of a DAS interrogator by comparing DAS recordings with conventional measurements in geophysics, including geophones, seismometers, and FBG strain sensors. Most importantly, the results suggest that the DAS measurements, approximately, represent ground deformation over a frequency range of 17 octaves, ranging from 1/3600 up to 60 Hz among four test sites, each with different fiber-ground coupling and source mechanisms. Although the instrument response is not exactly equal to 1, the results suggest that DAS may be used in conjunction with geophysical methods that rely not only on arrival times, but also on the waveforms, such as full-waveform inversion.

Potential errors in DAS-derived displacement amplitude estimates that result from incorrect phase-velocity estimates can be mitigated by incorporating strain or strain-rate measurements directly into geophysical workflows as observables, following the approach of Paitz *et al.* (2018) for noise interferometry.

With the wide range of emerging applications within the DAS community in seismology, there is a need to quantify the measurement properties of DAS interrogators and to link the observed waveforms to ground motion. This requires further comprehensive DAS instrument-response studies for different interrogators, fiber installations, and experiment setups.

Based on these results, we suggest the establishment of a standardized workflow for DAS experiments to estimate the properties of the instrument response and gather them in a community DAS response database that is publicly available. This database would help aggregate information on best practices for DAS measurements and could be utilized as quality control and on-site DAS calibration for each experiment individually. In addition, the influence of specific sites on the response can be better quantified, if more response studies are available. Therefore, new logistical challenges emerge,

including unified data and metadata-formats and an instrument-response standard similar to existing poles-and-zeros files for conventional sensors.

With more quantitative studies on DAS and the growing abundance of strain and strain-rate data in seismology, there is an urgent need to include these quantities into conventional seismological workflows. To better estimate the strain-response itself as opposed to a velocity-equivalent response, laboratory experiments under controlled and realistic conditions are required. This would not only mitigate potential errors in phase-velocity estimation or isolate systematic-coupling response characteristics, but could also reassure the quality of DAS measurements and potentially answer the question if instrument-response correction for DAS interrogators is required at all.

With a frequency range that many conventional seismometers may not compete with, DAS is in the process of revolutionizing the field of seismic data acquisition, especially in urban and environmental seismology.

DATA AND RESOURCES

The data from the Yverdon-les-Bains test site were collected in association with the INNOSUISSE Geothermal Chance of Success (GECOS) project and cannot be released to the public at this stage. The seismograms from the reference seismometer at the Grimsel test site (GTS) used in this study were accessed via ObsPy (Beyreuther *et al.*, 2010) from the European Integrated Data Archives (http://eida.ethz.ch) with the network and station code CH.GRIMS. The seismometer data from the Rhonegletscher experiment were collected via the 4D local glacier seismology network (doi: 10.12686/sed/networks/4d/), and are available via the web interface of the Swiss Seismological Service (http://arclink.ethz.ch/webinterface/) with the network and channel code RA52. Data from selected distributed acoustic sensing (DAS) channels from the Rhonegletscher installation, the GTS DAS earthquake recordings, the fiber-Bragg-grating (FBG) strain recordings and collocated DAS recordings are archived on ETH's Seismology and Wave Physics server. Access can be granted by the authors upon request. All websites were last accessed in May 2020. More detailed images of the waveforms from Figure 2 are available in Figures S1–S6 (available in the supplemental material to this article).

ACKNOWLEDGMENTS

The authors want to thank Editor-in-Chief Thomas Pratt, Editor Cezar I. Trifu as well as Reviewer Eileen Martin and one anonymous reviewer for reviews and comments to help improve this article.
Furthermore the authors would like to thank Nate Lindsey, Jonathan Ajo-Franklin, and Horst Rademacher for fruitful discussions on distributed acoustic sensing and instrument-response investigations. The authors also thank Swiss National Cooperative for the Disposal of Radioactive Waste (NAGRA), especially Rene Dorrer and Michael Treuhardt from the Grimsel test site (GTS) for their support and help with the experiments in their facilities. The authors want to thank Geo2x and Geothermal Exploration Chance Of Success (GECOS) for the fieldwork support in Yverdon-les-Bains and the Laboratory of Hydraulics, Hydrology and Glaciology at ETH Zürich (VAW) field crew from the Rhonegletscher experiment. The authors also thank Daniel Bowden for fieldwork support. This work would not have been possible without the help of everyone involved in the field logistics and data acquisitions. Furthermore, the authors thank Stoyan Nikolov, Andy Clarke, and Silixa for their ongoing support throughout all experiments.
Author Chalari works for the instrument manufacturer and served as a liason with the company during this work. The other authors and their institutions have no financial relationship with the company, and have no financial stake in patents for the instrumentation used in this study. The interrogator used in this study was previously purchased from Silixa. Silixa provided technical support for the discussed experiments. This work has been supported by the ETH Research Grants ETH-01 16-2 (PP) and ETH-06 16-2 (DG and Rhonegletscher experiment), by the Swiss National Science Foundation (SNSF) under Grant 200021_149143 (AF) and Grant PP00P2_18371 (FW), and by GECOS, a project co-funded by INNOSUISSE, Services Industriels de Geneve and GEO2X SA under Project Number 26728.1 PFIW-IW (PE and Yverdon-les-Bains experiment). The Grimsel experiments were part of effort of the Swiss Competence Center for Energy Research—Supply of Electricity (SCCER-SoE).

REFERENCES

Ajo-Franklin, J. B., S. Dou, N. J. Lindsey, I. Monga, C. Tracy, M. Robertson, V. R. Tribaldos, C. Ulrich, B. Freifeld, T. Daley, *et al.* (2019). Distributed acoustic sensing using dark fiber for near-surface characterization and broadband seismic event detection, *Sci. Rep.* **9,** no. 1, 1–14.

Becker, M. W., and T. I. Coleman (2019). Distributed acoustic sensing of strain at earth tide frequencies, *Sensors* **19,** no. 9, 1975.

Beyreuther, M., R. Barsch, L. Krischer, and J. Wassermann (2010). ObsPy: A Python toolbox for seismology, *Seismol. Res. Lett.* **81,** 47–58.

Daley, T. M., B. M. Freifeld, J. Ajo-Franklin, S. Dou, R. Pevzner, V. Shulakova, S. Kashikar, D. E. Miller, J. Goetz, J. Henninges, *et al.* (2013). Field testing of fiber-optic distributed acoustic sensing (DAS) for subsurface seismic monitoring, *The Leading Edge* **32,** no. 6, 699–706.

Daley, T. M., D. Miller, K. Dodds, P. Cook, and B. Freifeld (2016). Field testing of modular borehole monitoring with simultaneous distributed acoustic sensing and geophone vertical seismic profiles at Citronelle, Alabama, *Geophys. Prospect.* **64,** no. 5, 1318–1334.

Doetsch, J., V. Gischig, H. Krietsch, L. Villiger, F. Amann, N. Dutler, R. Jalali, B. Brixel, C. Roques, P. Giertzuch, *et al.* (2018). *Grimsel ISC experiment description*, *Technical Report*, ETH Zurich, doi: 10.3929/ethz-b-000310581.

Dou, S., N. Lindsey, A. M. Wagner, T. M. Daley, B. Freifeld, M. Robertson, J. Peterson, C. Ulrich, E. R. Martin, and J. B. Ajo-Franklin (2017). Distributed acoustic sensing for seismic monitoring of the near surface: A traffic-noise interferometry case study, *Sci. Rep.* **7,** no. 1, Article Number 11620.

Dziewoński, A. M., A. L. Hales, and E. R. Lapwood (1975). Parametrically simple Earth models consistent with geophysical data, *Phys. Earth Planet. In.* **10,** 12–48.

Fry, B., F. Deschamps, E. Kissling, L. Stehly, and D. Giardini (2010). Layered azimuthal anisotropy of Rayleigh wave phase velocities in the European Alpine lithosphere inferred from ambient noise, *Earth Planet. Sci. Lett.* **297,** 95–102.

Hartog, A. H. (2017). *An Introduction to Distributed Optical Fibre Sensors*, CRC Press, Boca Raton, Florida.

Jousset, P., T. Reinsch, T. Ryberg, H. Blanck, A. Clarke, R. Aghayev, G. P. Hersir, J. Henninges, M. Weber, and C. M. Krawczyk (2018). Dynamic strain determination using fibre-optic cables allows imaging of seismological and structural features, *Nat. Comm.* **9,** no. 1, 2509.

Krietsch, H., J. Doetsch, N. Dutler, M. Jalali, V. Gischig, S. Loew, and F. Amann (2018). Comprehensive geological dataset describing a crystalline rock mass for hydraulic stimulation experiments, *Sci. Data* **5,** Article Number 180269.

Kuvshinov, B. (2016). Interaction of helically wound fibre-optic cables with plane seismic waves, *Geophys. Prospect.* **64,** no. 3, 671–688.

Li, M., H. Wang, and G. Tao (2015). Current and future applications of distributed acoustic sensing as a new reservoir geophysics tool, *Open Petrol. Eng. J.* **8,** no. 1, 272–281.

Lindsey, N. J., E. Martin, D. Dreger, B. Freifeld, S. Cole, S. James, B. Biondi, and J. B. Ajo-Franklin (2017). Fiber-optic network observations of earthquake wavefields, *Geophys. Res. Lett.* **44,** no. 23, 11,792–11,799.

Lindsey, N. J., H. Rademacher, and J. B. Ajo-Franklin (2020). On the broadband instrument response of fiber-optic das arrays, *J. Geophys. Res.* **125,** e2019JB018145.

Martin, E., N. Lindsey, S. Dou, J. Ajo-Franklin, T. Daley, B. Freifeld, M. Robertson, C. Ulrich, A. Wagner, and K. Bjella (2016). Interferometry of a roadside das array in Fairbanks, AK, *SEG Technical Program Expanded Abstracts 2016*, Dallas, Texas, 19 October 2016,Society of Exploration Geophysicists, 2725–2729.

Martin, E. R., C. M. Castillo, S. Cole, P. S. Sawasdee, S. Yuan, R. Clapp, M. Karrenbach, and B. L. Biondi (2017). Seismic monitoring leveraging existing telecom infrastructure at the SDASA: Active, passive, and ambient-noise analysis, *The Leading Edge* **36,** no. 12, 1025–1031.

Martin, E. R., N. Lindsey, J. Ajo-Franklin, and B. Biondi (2018). Introduction to interferometry of fiber optic strain measurements, *EarthArXiv*, doi: 10.31223/osf.io/s2tjd.

Paitz, P., K. Sager, and A. Fichtner (2018). Rotation and strain ambient noise interferometry, *Geophys. J. Int.* **216,** no. 3, 1938–1952.

Singh, S., Y. Capdeville, and H. Igel (2019). Correcting wavefield gradients for the effects of local small-scale heterogeneities, *Geophys. J. Int.* **220,** no. 2, 996–1011.

Walter, F., D. Gräff, F. Lindner, P. Paitz, M. Knoepfli, M. Chmiel, and A. Fichtner (2020). Distributed acoustic sensing of microseismic sources and wave propagation in glaciated terrain, *Nat. Comm.* **11,** 2014–1723.

Wang, H. F., X. Zeng, D. E. Miller, D. Fratta, K. L. Feigl, C. H. Thurber, and R. J. Mellors (2018). Ground motion response to an M_L 4.3 earthquake using co-located distributed acoustic sensing and seismometer arrays, *Geophys. J. Int.* **213,** no. 3, 2020–2036.

APPENDIX

This Appendix includes Table A1.

Manuscript received 20 May 2020
Published online 20 October 2020

TABLE A1
Overview of the Experiments Discussed in This Article

Experiment and Date	Location	Investigated Signals and Frequency Range	Fiber Coupling	Reference Measurement
Hydraulic injection 2018/05/30	Grimsel test site	Signals due to increase in hydraulic pressure in the rock between 1/3600 and 1/200 Hz	Cemented in 70-meter-deep borehole. Measurements at a depth of 20 m	Strain from fiber-Bragg-grating collocated and cemented in the same borehole. Sensor: Micron Optics Inc. os3600 with 1 m base length
Earthquake recordings Fiji: 2018/08/19. Ionian Sea: 2018/10/25. Linthal: 2018/08/30	Grimsel test site Fiji: lat = −18.113°, lon = −178.153°, baz = 12°. Ionian: Lat = 37.506°, lon = 20.563°, baz = 130°. Linthal: Lat = 46.91°, lon = 8.93°, baz = 51°	Three different earthquake recordings with sources in Fiji (d = 16,800 km), in the Ionian Sea (d = 1300 km) and close to Linthal, Switzerland (d = 60 km). Signals ranging from 1/26 to 13 Hz. Only surface waves are considered here	Loose on concrete in a 60-meter-long tunnel going back and forth 24 times, with parts of the cable covered by gravel bags, parts covered by wooden blocks, parts taped to the ground and the most part loose on the ground	Velocity from permanent station CH.GRIMS of the Swiss Seismological Service, 50 cm next to cable. Streckeisen STS2 (third generation) with a Quanterra Q330HRS digitizer
Active seismic 2019/10/02	Yverdon-les-Bains	Active vibroseis sweeps from 12 to 150 Hz (with the main energy of the signals ranging from 20 to 40 Hz). Only surface waves considered here	Trenched in soil at a depth of around 30 cm. The length of the layout is 120 m and the fiber is going back and forth two times	Velocity from geophone array 2 m next to cable. Instruments: SM6 (14Hz) by INPUT/OUTPUT INC. with a Geometrics ES-3000 digitizer
Icequake recording 2019/03/23	Rhonegletscher	Icequake recording from a source around 100 m north of the fiber. Signal from 30 to 70 Hz	Trenched in snow at a depth between 2 and 20 cm over three sections of around 300 m each (triangle)	Three-component Lennartz 3D/BHs sensors, drilled 3 m into the ice below 2 m of snow cover. Digitizer: Nanometrics Centaur

An overview of the experiment locations is provided in Figure 2. For the locations, the latitude (lat), longutude (lon), and back azimuth (baz) of the surface-wave arrival are provided.